Engineering Structures 286 (2023) 116084

Contents lists available at ScienceDirect

Engineering Structures

journal homepage: www.elsevier.com/locate/engstruct

Strain driven mode-switching analytical framework for estimating flexural strength of RC box girders strengthened by prestressed CFRP plates with experimental validation

Yu Deng [a], Daoyuan Ling [a], Zhen Guo [a], Piti Sukontasukkul [b], Terry Y.P. Yuen [c], Simon H. F. Wong [d], Mark Adom-Asamoah [e], Suchart Limkatanyu [f], Chayanon Hansapinyo [g], Jack Banahene Osei [e], Jones Owusu-Twumasi [e], J.S. Kuang [h], Hexin Zhang [i,*]

[a] School of Civil Engineering and Architecture, Guangxi University of Science and Technology, Liuzhou 545006, China
[b] Construction and Building Materials Research Center, Department of Civil Engineering, King Mongkut's University of Technology North Bangkok, Bangkok 10800, Thailand
[c] Department of Civil Engineering, National Yang Ming Chiao Tung University, Hsinchu, Taiwan
[d] Department of Construction Technology and Engineering, Technological Higher Education Institute of Hong Kong, 20A Tsing Yi Road, Tsing Yi Island, New Territories, Hong Kong
[e] Department of Civil Engineering, Kwame Nkrumah University of Science and Technology, Kumasi, Ghana
[f] Department of Civil and Environmental Engineering, Faculty of Engineering, Prince of Songkla University, Songkhla 90112, Thailand
[g] Excellence Center in Infrastructure Technology and Transportation Engineering (ExCITE), Department of Civil Engineering, Chiang Mai University, Chiang Mai 50200, Thailand
[h] Department of Civil and Environmental Engineering, Hong Kong University of Science and Technology, Kowloon, Hong Kong
[i] School of Computing, Engineering and the Built Environment, Edinburgh Napier University, 10 Colinton Road, Edinburgh, Scotland EH10 5DT, UK

A R T I C L E I N F O

Keywords:
RC box girder
prestressed CFRP plate
Strengthening
Shear lag effect
Analytical model

A B S T R A C T

This paper presents a pioneering study that developed the first analytical model to analyse and design reinforced concrete (RC) box girders strengthened by prestressed CFRP plates. The proposed analytical model considered and addressed prestress loss, shear lag effect and failure modes under different design configurations at elastic, elastoplastic and plastic stages. An experimental study was also conducted to validate the proposed analytical model. The study was motivated by the increasing demand for the structural strengthening of aged and over-used hollow RC box girders in transport and other infrastructure systems, as well as the lack of previous attempts to incorporate prestressed CFRP plate strengthening for hollow RC beams. It is very common in many developing countries, the traffic flow increased dramatically due to the economic growth. The original design under-estimated the traffic loads. When demolition and re-building may not always be the best option, thus, strengthening and enhanced maintenance have become promising alternatives. But the lack of existing analytical models that can guide the engineers to analyse and design this type of structures effective, has become an urgent need from the industry. In the experimental study, eight box girders with different types, cross-section sizes, and prestress levels were prepared and tested. Two samples were preloaded to create damaged beams before strengthening to simulate the aged or over-used members. The experimental results are in good agreement with the analytical prediction. The proposed analytical framework provides a comprehensive yet practical method for designing the prestressed CFRP strengthened RC box girders in bending and laid the foundation for further studies on shear and torsion behaviours.

1. Introduction

RC box girder is one of the most common structural forms widely used in many infrastructures such as bridges, highway viaducts and many other transportation applications. Some RC box girders were constructed decades ago. Many of these decades-old RC box girder structures are still in use, but the traffic conditions have become much more demanding. Demolition and re-building may not always be the

* Corresponding author.
E-mail address: j.zhang@napier.ac.uk (H. Zhang).

https://doi.org/10.1016/j.engstruct.2023.116084
Received 12 September 2022; Received in revised form 24 March 2023; Accepted 1 April 2023
Available online 19 April 2023

best option, thus, strengthening and enhanced maintenance have become promising alternatives. The carbon fibre rod and plate strengthening are the most popular strengthening technologies due to their outstanding mechanical properties, corrosion resistance and the benefit of achieving increased strength after being prestressed [1–13]. Strengthening RC structures with prestressed CFRP rods and plates has become one of the engineers' favourite options. However, most previous studies have focused on RC beams with solid cross-sections. Due to analysis and modelling complexities, no previous study has considered hollow sections such as RC box girders. In this era where computer modelling of structures is revolutionising the structural engineering field, there is an industry-driven demand to develop an analytical model to support the computer-aided analyse and design of the prestressed CFRP rod or plate-strengthened RC box girder.

Several interesting research works related to solid cross-sections have been conducted before. Wight et al. [14] and Bansal et al. [15] reported their experimental studies on the performance of non-prestressed and prestressed CFRP sheets in strengthening large-scale prestressed concrete beams and RC girders. They found that the anchorage of the CFRP sheets at both ends plays a crucial role in the overall capacity of the structural members. Garden and Hollaway [16,17] and Li et al. [18] also investigated how the prestress levels and prestress loss influence the flexural capacity of the RC beams strengthened by the prestressed CFRP plates. Yang et al. [19] and Ahmed et al. [20] evaluated the flexural performance of the CFRP strengthened reinforced concrete members with different bonding and prestressing methods. Xue et al. [21], Emdad and Al-Mahaidi [22] conducted both experimental and theoretical analyses on RC beams strengthened with prestressed CFRP plates. They proposed an analytical model for estimating the prestress loss of CFRP plates, anti-cracking capacity, crack width and deflection of the strengthened reinforced concrete beams. Zhang [23] and Chi Han et al. [24] studied the flexural performance of the prestressed CFRP plate strengthened T-shaped beams and suggested that the high prestress level would lead to a higher ultimate capacity, better crack resistance and slower crack propagation. Täljsten [25], Deng and Lee [26] studied the peeling and shear stress between the glueing line using the numerical and experimental approaches. Woo et al. [27] and Yang et al. [28] investigated the flexural behaviour of prestressed CFRP plate strengthened RC beams and proposed the analytical equations for calculating the flexural capacity after strengthening. Chaallal et al. [29] studied and compared the performance of the embedded through-section (ETS) CFRP rod and externally bonded (EB) CFRP sheet. Peng et al. [30] designed a piece of pretensioning equipment for CFRP plate and conducted an experimental study on the flexural performance of rectangular RC beams strengthened with externally bonded prestressed CFRP plates. The experimental results suggest that the prestressed CFRP plate could significantly improve cracking resistance and yielding load and reduce the deformation at the serviceability limit state.

Prestressed CFRP plate has demonstrated its great potential in strengthening the new, aged or damaged RC structure. It has attracted significant research attention in recent years. However, all these previous works studied mainly the structural members with solid cross-sections such as rectangular or T-shaped RC beams. To the best of the authors' knowledge, i) no previous study has focused on structural members with a hollow section that is strengthened by the prestressed CFRP plates, such as RC box girders, which are widely used in many bridges, highway viaducts and many other transportation applications; Several current relevant standards: JTG/T J22-2008 [31], GB 50367-2013 [32], CECS 146-2003 [33], ACI 440.2R-02 [34] all have no specification for the analysis and design of the RC box girders strengthened by the prestressed CFRP plates. ii) no previous analytical model or study that could enable engineers to adopt this technology by providing a method for analysis and design of this type of structural members. However, for structures with hollow sections, the demand for structural maintenance and strengthening in case of ageing and deterioration is higher than the ones with solid cross-sections. Prestressed CFRP plate strengthening does provide a competitive approach for this purpose.

In this paper, an analytical study that focuses on the design theory and analysis principles for prestressed CFRP plate strengthened RC box girders is presented. The types of CFRP plates include the normal CFRP plate and the steel wired carbon fibre reinforced polymer (SWCFRP) plate. For the sake of convenience, both types of plates will be referred to as CFRP plate. The elastic–plastic behaviours were considered in these analytical models, and two different failure modes of the specimens were analysed to formulate the flexural capacity with the prestress losses considered.

The analytical results from the proposed model were validated using the experimental study conducted on RC box girders strengthened by prestressed CFRP plates. A total of eight RC box girders were manufactured and tested, as shown in Table 1. Two of the eight samples were preloaded to partially damaged/cracked status. The damage level was measured using the strain of tensile reinforcement at 60% and 80% of the yielding strain. The structural performances of these samples were evaluated using a four-point bending test.

The analytical results agree with the experimental outcomes, proving that the proposed analytical models are adequate for practical engineering applications.

2. Experimental validation

2.1. Specimen design

Limited by the laboratory space constraints and the loafing capacity of the test equipment, the following dimensions were used in the design of the box girders: total length of 3.6 m, upper and lower flange width of 600 mm and 400 mm, respectively, and a total height of 380 mm, and web thickness of 60 mm. The thickness of the upper and lower flanges was 80 mm, and a thickness of 20 mm was used as the concrete cover for the reinforcement. The concrete strength class of C40 (40 MPa) was used

Table 1
Designation and design parameters of specimen beams.

Serial number	Section area (mm^2)	Degree of damage (strain value of tensile reinforcement)	Tension control stress	Carbon plate material
DBL	/	/	/	/
JGL1-3P	50 × 2	/	30%	Common carbon fibre plate
JGL1-4P	50 × 2	/	40%	Common carbon fibre plate
JGL2-4P	50 × 3	/	40%	Common carbon fibre plate
JGL3-3P	50 × 3	/	30%	Steel based carbon fibre plate
JGL3-4P	50 × 3	/	40%	Steel based carbon fibre plate
SSL1A-3P	50 × 2	60% of the yield strain	30%	Common carbon fibre plate
SSL1B-4P	50 × 2	80% of the yield strain	40%	Common carbon fibre plate

Note: DBL represents the unreinforced contrast beam; JGL - CFRP strengthened beam; SSL - CFRP strengthened beam with some degree of damage; 1 - common CFRP board with a section area of 50 mm × 2 mm; 2 - ordinary CFRP board with a section area of 50 mm × 3 mm; 3 - steel-based CFRP plate with a section area of 50 mm × 3 mm mixed with high-strength steel wire; 3P - the tensile stress is 30% of that of ordinary carbon plates; 4P - the tensile stress is 40% of that of ordinary carbon plates.

in the design of the samples. Also, the number/diameter of the tension and compression reinforcements are 4No. of Φ6 (6 mm), 5 No. of Φ10 (10 mm) HRB400 steel reinforcement, respectively. The number/diameter of the longitudinal web reinforcement on both sides is 2 No. Φ8 (8 mm) HRB400 steel reinforcement, respectively. The shear stirrup within the pure bending section (1 m length) was Φ10 (10 mm) at 200 mm centre-to-centre, while within the two shear-bending sections (1.2 m length each), the stirrup was Φ10 (10 mm) at 100 mm centre-to-centre. The details of the sample beam and the test setup are shown in Fig. 1.

The CFRP plates were provided by Liuzhou OVM Machinery Co, Ltd (OVM). Three types of CFRP plates were used in this study. For standard/ordinary CFRP plates, model OVM.CFP50-2 and OVM.CFP50-3 were used, while GJ.CFP50-3 model was used for SWCFRP plates.

Furthermore, Lica-131A/B carbon fibre composite impregnated adhesive (fibre composite structural adhesive) was also used in this study. The Lica-131A/B was manufactured by Nanjing Hitech Composite Material Co., LTD. Table 1 shows the detailed specification of all the samples. Samples SSL1A-3P and SSL1B-4P were partially damaged by preloading them until 60%, and 80% of their steel rebar yielding tensile strength was obtained, respectively. The yield tensile strength was measured by the tensile stresses in the tension reinforcement. In other words, these two samples were loaded until 60%, and 80% of their rebars' yielding strength was reached, respectively. The preloading was done to create a pre-damaged (cracked) box beam before they were strengthened by the CFRP plates. The mechanical properties of the materials are listed in Table 2 and Table 3.

The pre-stressing and installation of CFRP plates were conducted with the facilities in Liuzhou OVM Machinery Co., LTD, following the procedure specified below:

(1) Mark the anchorage zone at the central line on the bottom of the box girder.
(2) Locate the centre of the anchor bolts and drill the holes with the proper size and depth according to the installation instruction of the bolts.
(3) Install the anchor plates using chemical anchor bolts.
(4) Check the surface to ensure no damage on the carbon plate, then install the anchor at the tension and reaction ends. During installation, the contact surface of the CFRP plate should be cleaned with alcohol or other cleaning agents specified by the manufacturer before applying the adhesive.
(5) Two 5 mm × 3 mm resistance strain gauges are installed along the longitudinal direction of the CFRP plate to monitor the stress of the carbon fibre plate during the prestressing and test stages later.
(6) CFRP plates are prestressed in five stages from 0 to 20%, then 40%, 60%, 80% and 100% of the control tension stress, σ_{con}. At each stage, the tension force was held for 3 min. The tension

Table 2
Mechanical properties of materials used in this study.

Material	Elasticity modulus/GPa	Tensile strength/MPa	Compressive strength/MPa	
Concrete C40	33.5	2.85	46.8	
Reinforcement	Φ8	200	465	/
	Φ10	200	468	/
	Φ20	200	470	/
Ordinary carbon plate	50 × 2	≥160	≥2400	/
	50 × 3	≥160	≥2400	/
Steel wire carbon plate	50 × 3	≥160	≥1466	/

Table 3
Basic parameters of adhesive used in this study.

Building structure adhesive	Compressive strength/MPa	Tensile bond strength with concrete/MPa	Standard value of tensile shear strength/MPa
Lica-131A/B	92	4.2 With C50 concrete bonding failure	27

Table 4
Table of control tension loads for CFRP tension process.

Carbon plate level			0.2	0.4	0.6	0.8	1.0
50 × 2/ $0.3f_u$	Ordinary carbon plate	Load/ kN	14.4	28.8	43.2	51.6	72
50 × 2/ $0.4f_u$	Ordinary carbon plate	Load/ kN	19.2	38.4	57.6	76.8	96
50 × 3/ $0.3f_u$	Ordinary carbon plate	Load/ kN	21.6	43.2	64.8	86.4	108
50 × 3/ $0.4f_u$	Steel wire carbon plate	Load/ kN	28.8	57.6	86.4	115.2	144

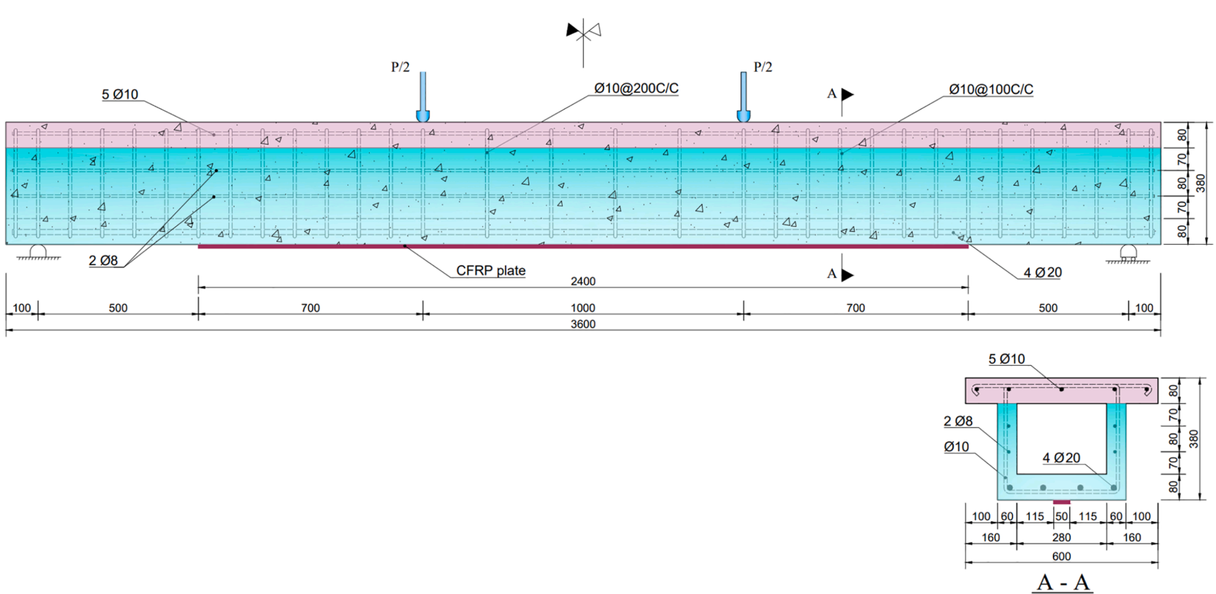

Fig. 1. Test beam loading diagram and reinforcement design.

(prestressing) forces required for each stage are shown in Table 4, and the schematic diagram of the tensioning device is shown in Fig. 2a and b.

(7) Brush the well-mixed adhesive on the surfaces of the concrete and the CFRP plate. The adhesive layer should be evenly applied on the concrete surface and 20–30 mm wider than the width of the CFRP plate. The adhesive should be applied to form a thicker layer in the middle and thinner at both edges. The adhesive layer should be around 1.5–2.0 mm thick on average.

(8) After applying the adhesive on both sides, press the CFRP plate gently onto the concrete and align it with the pre-set position. Use the rubber roller to press the CFRP plate's whole surface evenly. The excessive adhesive will be squeezed out from the two sides of the CFRP plate.

(9) The samples should be cured for 14 days in an isolated environment. Any vibration or movement could reduce the bonding strength.

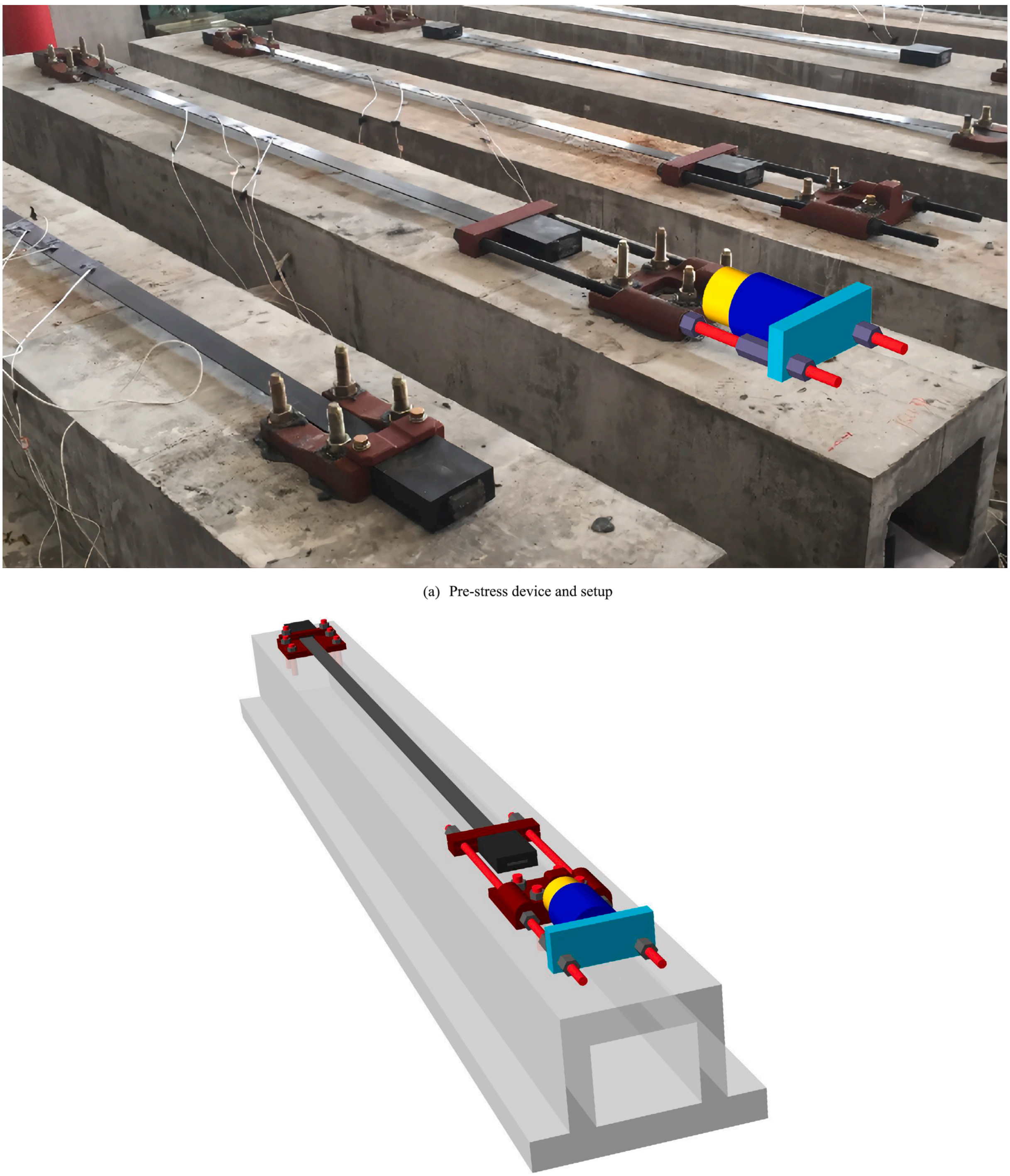

(a) Pre-stress device and setup

(b) Schematic illustration of the hydraulic prestress device and setup

Fig. 2. Details of pre-stress device and test setup.

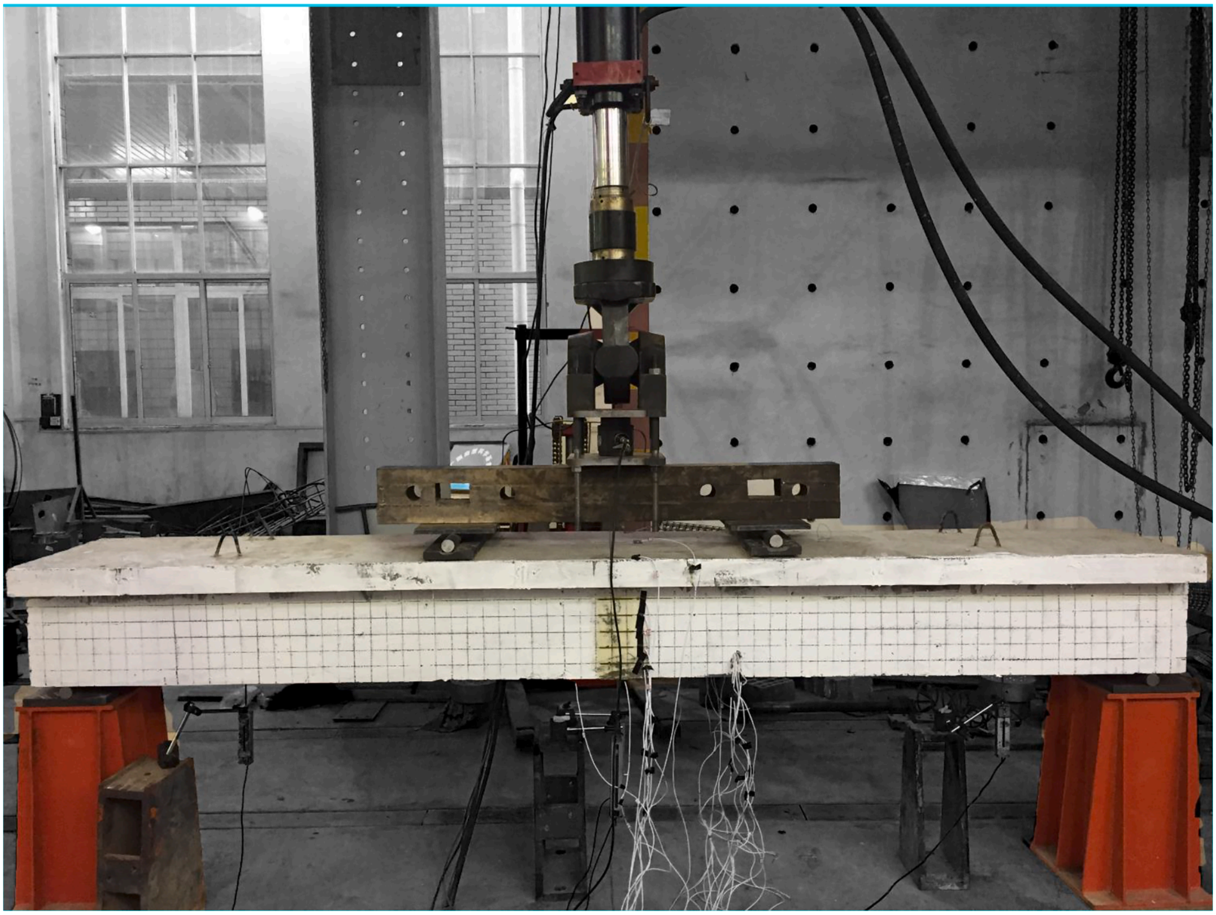

(c) Test setup

Fig. 2. (*continued*).

2.2. Test procedure

The sample was tested on MTS 50 T or 100 T hydraulic Servo System. The loading was spread through a 1-metre-long steel beam that rested on two rods with 15 mm thick spreading plates to ensure an even loading distribution (Fig. 2c). The pure bending and shear-bending zones are 1 m and 1.2 m long, respectively.

Displacement transducers were located under the two spread loading points, above the two supports and under the middle point of the beam. A 70 T load cell was installed and located at the central loading point. All the strain gauges, load cells and displacement transducers were connected to Yangzhou Jingmin JM-3813 Data Acquisition System (DAS). The test procedure is specified below:

(1) All samples were preloaded to 10% of the estimated value of the crack load and then returned to zero to check all the sensors and DAS.
(2) The load was applied at 5kN incremental steps until the first crack was observed. The loads were held for 10 min at each step to allow for sample inspection.
(3) After the first crack and before the maximum crack width reached 0.5 mm, the loading was applied at 10kN each step, with a 10-minute hold for each step.
(4) After the maximum crack width of 0.5 mm was reached, the load was increased steadily until the rupture.
(5) The sample was slowly and steadily unloaded while observing their behaviours during the unloading process.

3. Experimental results

3.1. Loss of prestress

Table 5 shows the average prestress loss of the prestressed CFRP plate from the strain gauges. The prestressing stress control was managed by a synchronised jacking system which has been proven in practical engineering operations and provided reliable stress control during the prestressing. The tensile strain was monitored daily after the prestress tensioning was released. In the first 15 days, the strain of the CFRP plate decreased significantly, but it remained constant beyond the 15 days, and the corresponding prestress loss was calculated accordingly. A comparison between the analytical and the experimental prestress loss is provided in the following section.

3.2. Estimation of prestress loss

The prestress loss was estimated based on the framework proposed in the literature [35,36], together with the parameters obtained from the experimental results in this study. Three key factors were considered:

(1) Prestress loss σ_{l1} is caused by shrinkage of prestressing carbon fibre plate and deformation of the tensioned end anchor. The anchoring tool independently developed by Liuzhou OVM Machinery Co., LTD was used as the anchoring device. Due to the gap between the anchoring tool and the nut, shrinkage of the prestress CFRP plate and deformation of the anchor will occur, and the prestress loss can be calculated as follows:

$$\sigma_{l1} = \frac{a}{l_f} E_f \tag{1}$$

Table 5
The comparison of experimental and analytical results of the total prestress loss of CFRP.

Specimen number	Tensioned microstrain $/10^{-6}$	Test microstrain (15d) $/10^{-6}$	Measured strain reduction $/10^{-6}$	Measured value of total prestress loss /MPa	Analytical predictions of prestress loss /MPa	Measured value/ Analytical value
JGL1-3P	5725	4340	1385	221.54	203.26	1.09
JGL1-4P	6164	4800	1364	218.21	208.01	1.05
JGL2-4P	7877	6426	1451	232.14	213.23	1.09
JGL3-3P	7418	6100	1318	210.87	199.69	1.06
JGL3-4P	7190	6005	1185	189.53	202.3	0.94
SSL1A-3P	5844	4383	1461	233.71	203.26	1.15
SSL1B-4P	6282	4851	1431	228.92	208.01	1.10

where a is the deformation value of the prestressed carbon fibre plate inner shrinkage and tensioned end, anchor, according to Table 10.2.2 in the Design of Concrete Structures code (GB50010-2010), a = 3 mm was selected; l_f is the pasted length of the CFRP plate which is chosen as 2.55 m in this research, and E_f is the modulus of elasticity of the CFRP plates.

(2) Prestress loss σ_{l2}, caused by stress relaxation of prestressed CFRP plates, the specified formula is as follows:

$$\sigma_{l2} = \frac{(1-\chi)\sigma_{con}}{100} \tag{2}$$

where:

$$\chi = 0.2756\sigma_{con}/f_u - 0.083$$

Here f_u is the tensile strength of the CFRP plate; σ_{con} is the tension control stress of the CFRP plate.

(3) Prestress loss σ_{l3}, caused by elastic compression and orifice friction of prestressed CFRP plates, can be defined as:

$$n_1 = \frac{E_f}{E_c} \tag{3}$$

$$\sigma_{l3} = n_1\sigma_{con}A_f\left(\frac{1}{A_0} + \frac{e_p^2}{I_0}\right) \tag{4}$$

where:

E_c is the elastic modulus of concrete.

E_f is the Elastic modulus of the CFRP plate.

A_f is the cross-sectional area of the prestressed CFRP plate.

A_0 is the section area of the whole specimen after conversion.

σ_{con} is the prestress design value of the CFRP plate. In this paper, the value is 2400 MPa.

e_p is the distance between the beam section tension zone's edge and the transformed section's gravity centre.

I_0 is the inertia moment of the transformed section.

The effective prestress value of the CFRP plate σ_{pe} can be calculated from the above losses:

$$\sigma_{pe} = \sigma_{con} - \sigma_{l1} - \sigma_{l2} - \sigma_{l3} \tag{5}$$

The experimental and analytical results of the prestress loss are in good agreement, as summarised in Table 5.

4. Flexural capacity of the box girder

4.1. Influencing factors of flexural capacity

The failure mode of the control beam DBL (as shown in Fig. 3a) is a typical bending failure. In this failure mode, the concrete in the compression zone is crushed after the tensile reinforcement yield. The CFRP strengthened samples, except one sample, JGL2-4P (Fig. 3d), and all the other samples: fJGL1-3P and JGL1-4P (Fig. 3b and Fig. 3c, none steel wired CFRP), JGL3-3P and JGL3-4P (Fig. 3e and Fig. 3f, steel wired CFRP), and SSL1A-3P and SSL1B-4P (Fig. 3g and Fig. 3h, pre-cracked/damaged beams strengthened by CFRP), all failed in pure bending. Cracks appeared in the mid-span, and the prestressed CFRP plates broke into strings and were pulled apart. In the test beam JGL2-4P (Fig. 3d), the concrete failed by crushing in the compression zone.

Fig. 4 shows the load–deflection curve of each sample. The deflection of all strengthened beams under the same load is smaller than that of the control beam (DBL). In the early loading stages, each test beam deflection was similar. While the load was increased, the reinforcement in the tensile zone yielded, and the deflection of beam DBL increased rapidly. However, the deflection of the strengthened beams, supported by the prestressed CFRP plate, increased relatively small. Fig. 5 shows the load–strain curves of carbon plates for each specimen beam.

A comparison of members SSL1A-3P, JGL1-3P, SSL1B-4P and JGL1-4P revealed that the deflection of beams strengthened after the damage is less than the ones directly strengthened with the same carbon fibre plate and other design configurations.

Table 6 summarises the amount of reinforcement, control prestress/tension stress, crack load, yielding load, ultimate load and strain of the carbon fibre plate before rapture for all samples. Compared with the control beam, the cracking load, yield load, and ultimate load of the strengthened beams significantly increased, ranging from 85.7% to 134.5%, 44.2% – 72.1% and 42.5% – 72.3%, respectively. Comparing the test beams JGL1-3P and JGL1-4P (or JGL3-3P and JGL3-4P) with the same amount of reinforcement, an increase in prestress level leads to an increased crack load, yield load and ultimate load of JGL1-4P (or JGL3-4P) by 10.9% (3.1%), 2.8% (2.3%) and 3.5% (2%), respectively. Comparing JGL1-4P and JGL2-4P, which have the same degree of prestressing, the crack load, yield load and ultimate load of JGL2-4P all increased by 13.9%, 16.1% and 16.8%, respectively.

JGL2-4P and JGL3-4P are strengthened with SWCFRP. With the same design configuration, the cracking load, yield load, and ultimate load were 7.2%, 6.9%, and 6.4% lower, respectively, than that of CFRP strengthened samples. The high-strength steel wires in the SWCFRP plate fractured before the carbon fibres, causing the uneven stress redistribution within the CWCFRP plate and leading to an earlier failure. However, considering the cost of the SWCFRP plates, it is still a cost-efficient option in practical applications.

Comparing beam JGL1-3P, JGL1-4P and pre-cracked/damaged beam SSL1A-3P and SSL1B-4P with a similar configuration, the yield load and ultimate load of the normal beams are not significantly different from those pre-cracked/damaged beams. The yield and ultimate load of the pre-cracked and damaged beams are only 6.0%– 6.5% and 0.7% – 4.5% smaller, respectively. The slightly larger variation in the ultimate load is caused by the different levels of final strain when the CFRP plates fail.

The experimental results revealed that the flexural capacity of the RC box girder was significantly increased after being strengthened by the prestressed CFRP plate. Both the size of the CFRP cross-section and the level of prestressing can increase the RC box girder's flexural capacity, but the CFRP cross-section's size has a higher impact on the overall flexural capacity. In a similar configuration, the normal and pre-cracked beams have small differences in flexural capacity after being strengthened by the CFRP plate. It proves that this technology has good potential in structural repair as well.

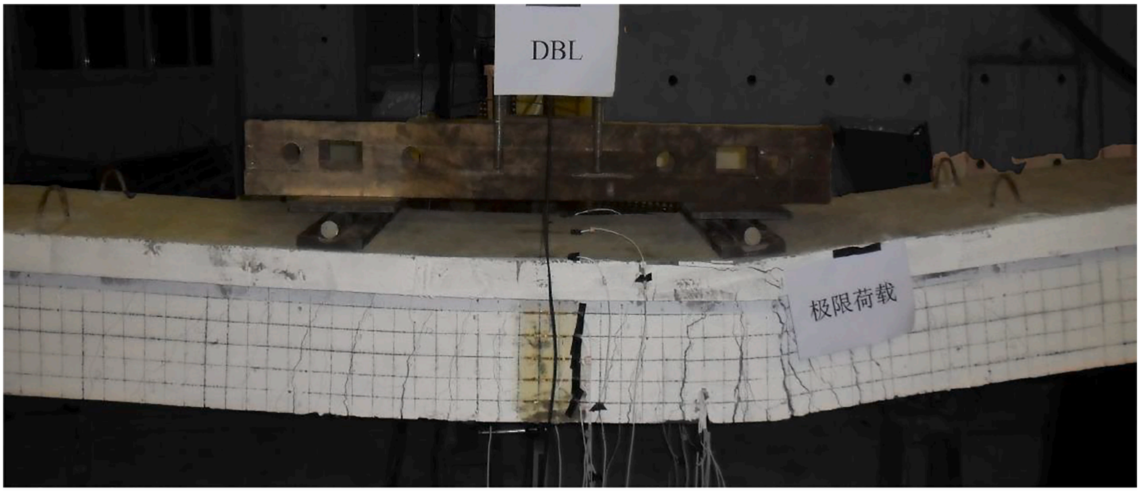

（a）DBL

（b）JGL1-3P

（c）JGL1-4P

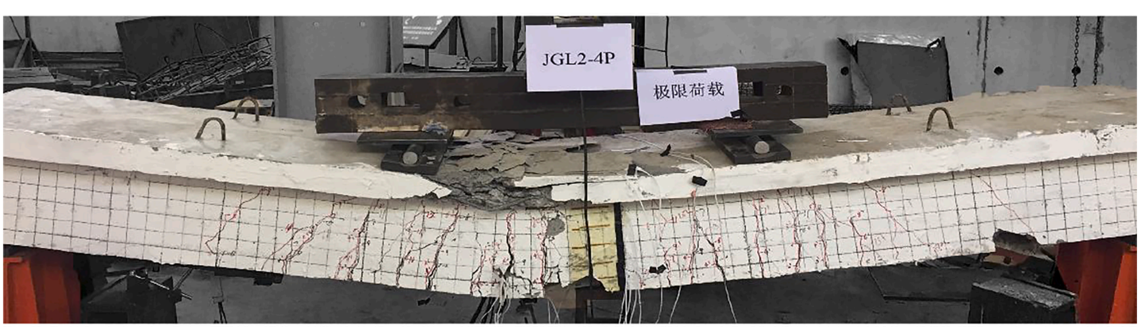

（d）JGL2-4P

Fig. 3. Failure characteristics of the beam specimens.

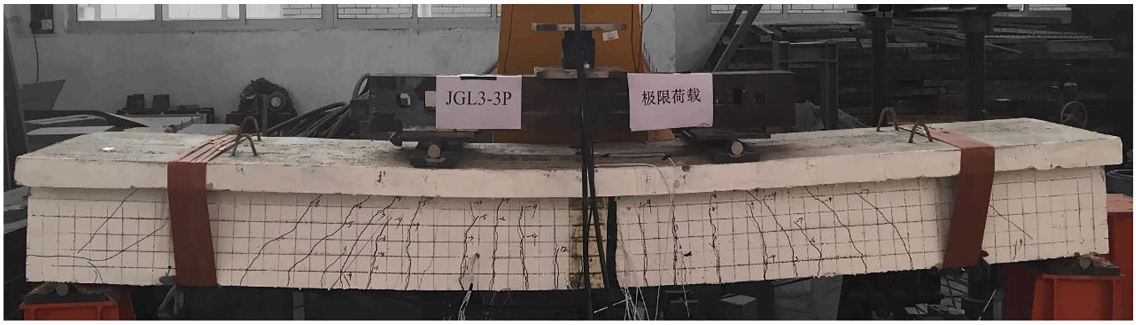

(e) JGL3-3P

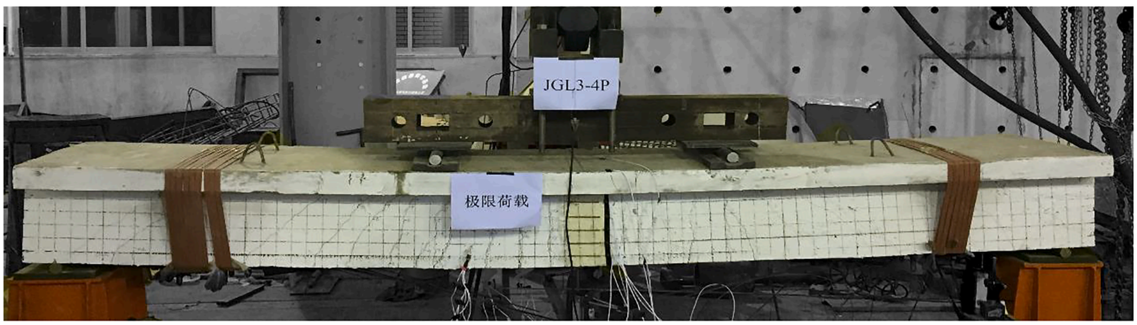

（f）JGL3-4P

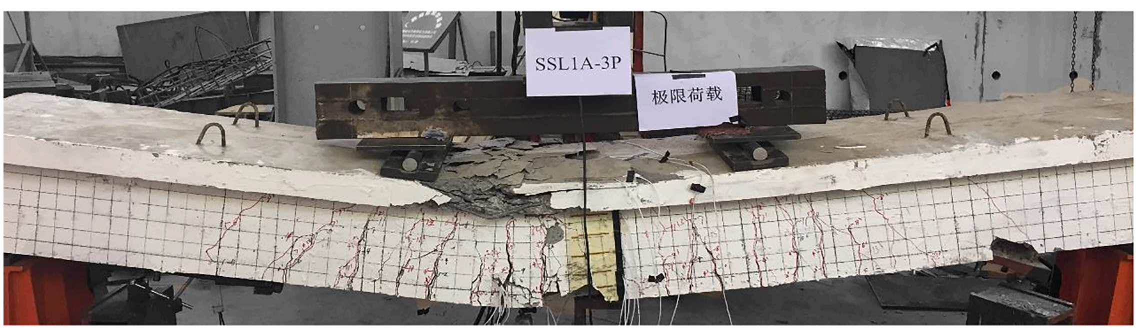

（g）SSL1A-3P

（h）SSL1B-4P

Fig. 3. (*continued*).

4.2. Calculation of flexural capacity

This section develops an analytical framework for estimating the CFRP strengthen RC box girders' flexural capacity. The proposed analytical framework/model is based on the sequence of first component (i.e., concrete, reinforcement and CFRP plate) failure to switch the mode of analysis to accommodate different design parameters such as dimensions of the cross-section, reinforcement ration, prestress level, and prestress losses. The mode-switching is based on the strain distribution within the cross-section that signalling the corresponding failure mode. The proposed framework/model also considered the thin-walled theory and two scenarios, with and without shear lag, and their associated three failure modes are considered.

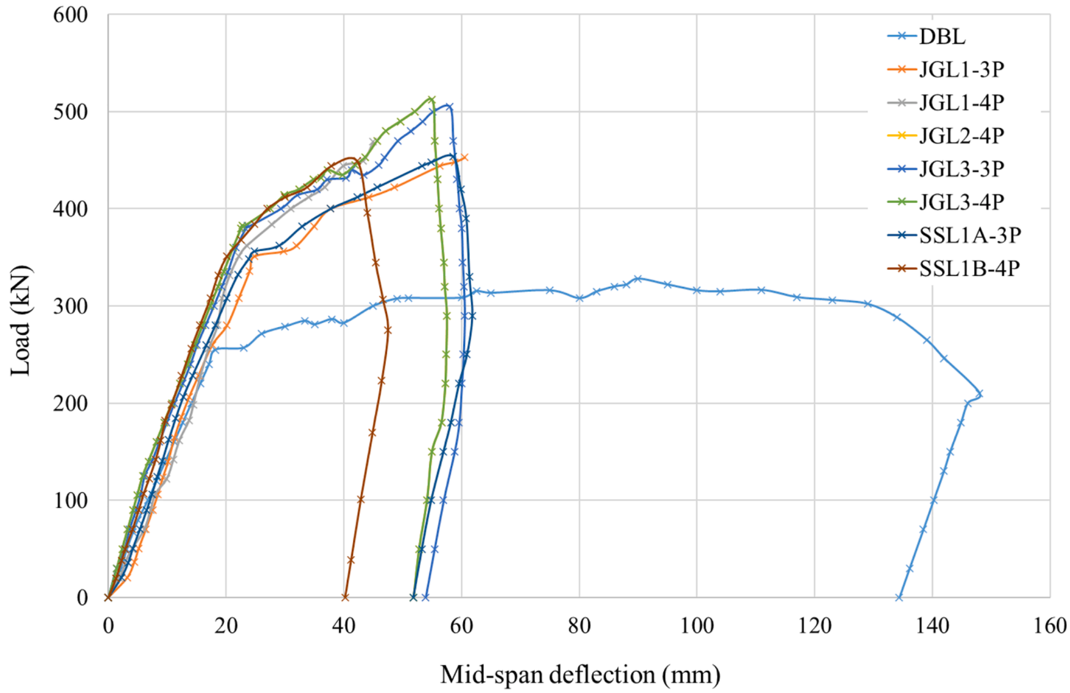

Fig. 4. Load-deflection curves of specimen beams.

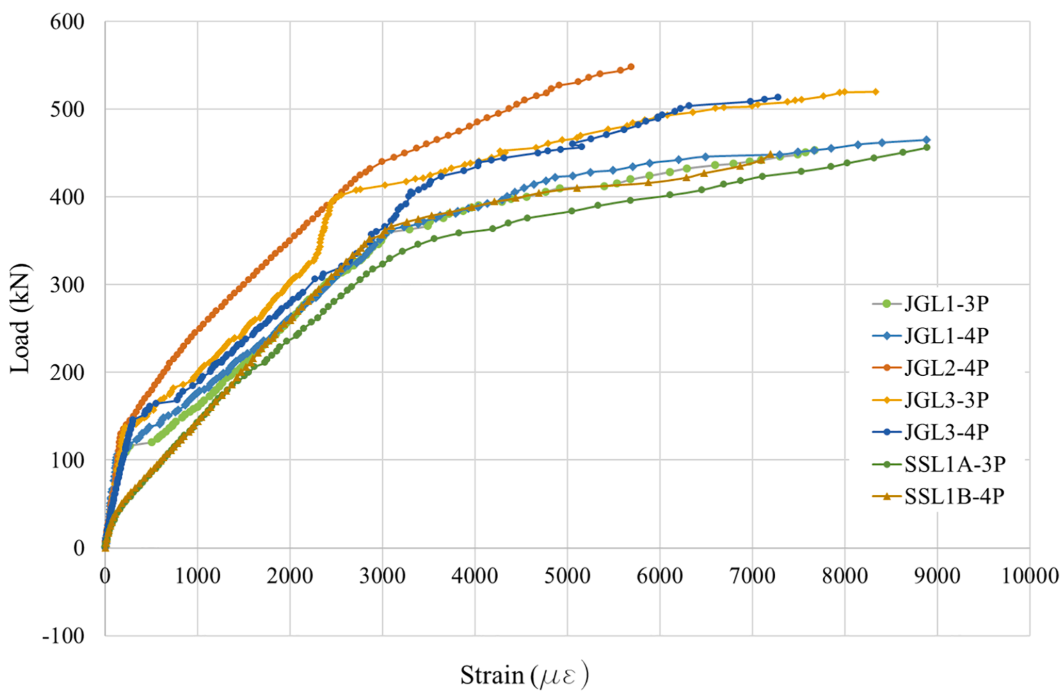

Fig. 5. Load-strain curves of carbon plates for each specimen beam.

4.2.1. Flexural capacity without considering the shear lag effect

Fig. 6 shows the cross-section of the RC box beam and the strain and stress distributions under bending but without considering the shear lag effect. Three different failure modes are considered.

i) failure mode 1

When the steel bar yields, the concrete is not crushed, while the CFRP plate reaches the ultimate tensile strain and breaks. Interpreting this condition to strain status, we have, $\varepsilon_c < \varepsilon_{cu}$, $\varepsilon_s > \varepsilon_y$, $\varepsilon_f = \varepsilon_{fu} - \varepsilon_i = \varepsilon_{fbu}$, assuming plane sections remain plane, have:

$$\varepsilon_s = \frac{h_0 - x_c}{h - x_c}\varepsilon_{fbu} \tag{6}$$

$$\varepsilon_s^{'} = \frac{x_c - a_s^{'}}{h - x_c}\varepsilon_{fbu} \tag{7}$$

$$\varepsilon_c = \frac{x_c}{h - x_c}\varepsilon_{fbu} \tag{8}$$

In this case:

Table 6
Summary of test results.

Number	Amount of reinforcement /mm^2	Tension control stress	Crack load /kN	α_{cr}	Yielding load /kN	α_y	Ultimate load /kN	$\alpha_{\max}$	Carbon fibre plate strain/10^{-6}	Type of failure mode
DBL	/	/	60.0	1.00	251	1.00	318	1.00	/	Concrete in compression zone is crushed.
JGL1-3P	50 × 2	30%f$_u$	111.4	1.86	362	1.44	453	1.42	7670	CFRP plate is pulled apart.
JGL1-4P	50 × 2	40%f$_u$	123.5	2.06	372	1.48	469	1.47	8879	CFRP plate is pulled apart.
JGL2-4P	50 × 3	40%f$_u$	140.7	2.34	432	1.72	548	1.72	5689	Concrete in compression zone is crushed.
JGL3-3P	50 × 3	30%f$_u$	127.2	2.12	395	1.57	505	1.59	8333	CFRP plate is pulled apart.
JGL3-4P	50 × 3	40%f$_u$	131.2	2.19	404	1.61	515	1.62	7276	CFRP plate is pulled apart.
SSL1A-3P	50 × 2	30%f$_u$	/	/	340	1.35	450	1.42	8893	CFRP plate is pulled apart.
SSL1B-4P	50 × 2	40%f$_u$	/	/	351	1.40	449	1.41	7199	CFRP plate is pulled apart.

Note: α_{cr}、α_y、$\alpha_{\max}$ respectively represent the ratio of cracking load, yield load and maximum bearing capacity of each beam after reinforcement to the corresponding value of contrast beam DBL.

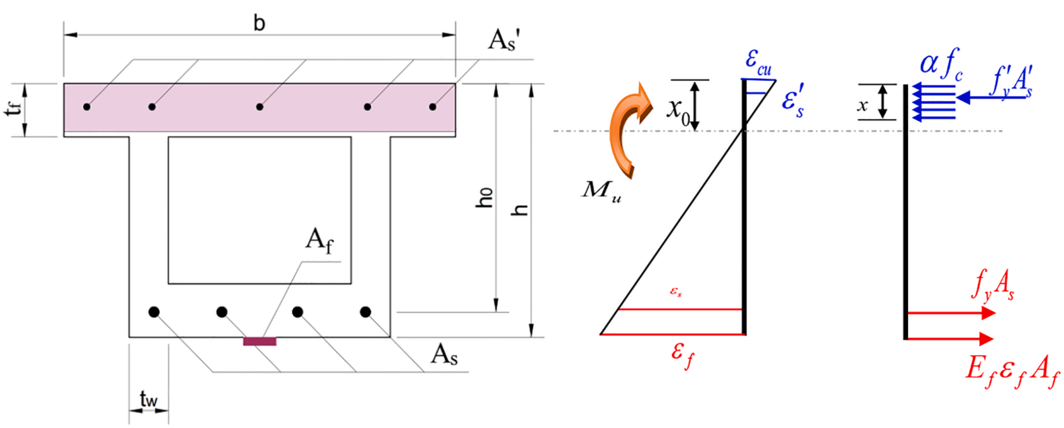

Fig. 6. Flexural capacity calculation of box girder section without considering shear hysteresis effect.

$$\sigma_s = \frac{f_u - f_y}{\varepsilon_{su} - \varepsilon_y}\varepsilon_s + \left(f_y - \frac{f_u - f_y}{\varepsilon_{su} - \varepsilon_y}\varepsilon_y\right) = f_y + \frac{f_u - f_y}{\varepsilon_{su} - \varepsilon_y}\left(\varepsilon_s - \varepsilon_y\right) \tag{9}$$

The equation of equilibrium of the internal forces in a horizontal direction is:

$$F_c + E_s^{'}\varepsilon_s^{'}A_s^{'} = \left(\sigma_{pe} + \varepsilon_{ce}E_f + \varepsilon_{fbu}E_f\right)A_f + \sigma_s A_s \tag{10}$$

(a) When $\varepsilon_c < \varepsilon_0$, by substituting Eqs. (6), (7), (8) and (9) into the equilibrium equation, Eq. (10), the expression can be simplified to the form $Ax_c^3 + Bx_c^2 + Cx_c + D = 0$. The approximate solution of the equation, solved by the Newton iteration method $x_{k+1} = x_k - \frac{f(x_k)}{f'(x_k)}$, can be obtained after 3–4 iterations to generate a more accurate solution, wherein:

$$A = \frac{b\sigma_0\varepsilon_{fbu}(\varepsilon_{fbu} + 3\varepsilon_0)}{3\varepsilon_0^2}$$

$$B = E_s^{'}A_s^{'}\varepsilon_{fbu} - \frac{b\sigma_0\varepsilon_{fbu}}{\varepsilon_0} + \frac{f_u - f_y}{\varepsilon_{su} - \varepsilon_y}\varepsilon_{fbu}A_s + q$$

$$C = -\frac{f_u - f_y}{\varepsilon_{su} - \varepsilon_y}\varepsilon_{fbu}A_s(h_0 + h) - 2hq - E_s^{'}A_s^{'}\varepsilon_{fbu}(a_s^{'} + h)$$

$$D = \frac{f_u - f_y}{\varepsilon_{su} - \varepsilon_y}\varepsilon_{fbu}A_s h_0 h + E_s^{'}A_s^{'} + h^2 q + E_s^{'}A_s^{'}a_s^{'}\varepsilon_{fbu}hq$$
$$= \left(\sigma_{pe} + \varepsilon_{ce}E_f + \varepsilon_{fbu}E_f\right)A_f + \left(f_y - \frac{f_u - f_y}{\varepsilon_{su} - \varepsilon_y}\varepsilon_y\right)A_s$$

(b) When $\varepsilon_c > \varepsilon_0$ $\varepsilon_c = \varepsilon_{cu}$ the formula can be simplified to give $Ax_c^3 + Bx_c^2 + Cx_c + D = 0$, then the solution of the equation is:

$$x_c = \frac{-B - \sqrt{B^2 - 4AC}}{2A}$$

wherein:

$$A = \frac{b\sigma_0(3\varepsilon_{fbu} + \varepsilon_0)}{3\varepsilon_{fbu}}$$

$$B = -\frac{b\sigma_0 h\varepsilon_0}{3\varepsilon_{fbu}} - \frac{f_u - f_y}{\varepsilon_u - \varepsilon_{sy}}\varepsilon_{fbu}A_s - q - E_s^{'}A_s^{'}\varepsilon_{fbu}$$

$$C = -\frac{f_u - f_y}{\varepsilon_{su} - \varepsilon_y}\varepsilon_{fbu}A_s h_0 + \frac{b\sigma_0\varepsilon_0 h^2}{3\varepsilon_{fbu}} + hq - E_s^{'}A_s^{'}\varepsilon_{fbu}a_s^{'}q$$
$$= \left(\sigma_{pe} + \varepsilon_{ce}E_f + \varepsilon_{fbu}E_f\right)A_f + \left(f_y - \frac{f_u - f_y}{\varepsilon_{su} - \varepsilon_y}\varepsilon_y\right)A_s$$

The ultimate flexural capacity is obtained by substituting x_c the conditions of (a) and (b) into the following equation:

$$M_u = \left(\sigma_{pe} + \varepsilon_{ce}E_f + \varepsilon_{fbu}E_f\right)A_f\left(h - \frac{x_c}{2}\right) + \sigma_s A_s\left(h_0 - \frac{x_c}{2}\right)$$
$$= \left(\sigma_{pe} + \varepsilon_{ce}E_f + \varepsilon_{fbu}E_f\right)A_f\left(h - \frac{x_c}{2}\right) + \left[f_y + \frac{f_u - f_y}{\varepsilon_{su} - \varepsilon_y}\left(\varepsilon_s - \varepsilon_y\right)\right]A_s\left(h_0 - \frac{x_c}{2}\right) \tag{11}$$

ii) failure mode 2

When the steel bar yields and the CFRP plate has not reached the tensile strain limit yet, the concrete in the compression zone is crushed and reaches its limit. Interpreting this condition to strain status, we have $\varepsilon_s > \varepsilon_y$ $\varepsilon_f < \varepsilon_{fbu}$ $\varepsilon_c = \varepsilon_{cu}$ the following equation can be obtained from the plane section assumption:

$$\varepsilon_s = \frac{h_0 - x_c}{x_c}\varepsilon_{cu} \tag{12}$$

$$\varepsilon_s' = \frac{x_c - a_s'}{x_c}\varepsilon_{cu} \tag{13}$$

$$\varepsilon_c = \frac{x_c}{h - x_c}\varepsilon_{cu} \tag{14}$$

When:

$$\sigma_s = \left(f_y - \frac{f_u - f_y}{\varepsilon_{su} - \varepsilon_y}\varepsilon_y\right) + \frac{f_u - f_y}{\varepsilon_{su} - \varepsilon_y}\varepsilon_s = \frac{f_u - f_y}{\varepsilon_{su} - \varepsilon_y}\left(\varepsilon_s - \varepsilon_y\right) + f_y \tag{15}$$

The equation of equilibrium of the internal forces in a horizontal direction is:

$$F_c + E_s'\varepsilon_s'A_s' = \left(\sigma_{pe} + \varepsilon_{ce}E_f + \varepsilon_f E_f\right)A_f + \sigma_s A_s \tag{16}$$

Substituting Eqs. (12), (13), (14) and (15) into the equilibrium equation, Eq. (16), the expression can be simplified into the form $Ax_c^3 + Bx_c^2 + Cx_c + D = 0$, and the solution of the equation can be obtained:

$$x_c = \frac{-B - \sqrt{B^2 - 4AC}}{2A}$$

where:

$$A = \frac{b\sigma_0(3\varepsilon_{cu} + \varepsilon_0)}{3\varepsilon_{cu}}$$

$$B = E_s'A_s'\varepsilon_{cu} + \frac{f_u - f_y}{\varepsilon_u - \varepsilon_y}\varepsilon_{cu}A_s + (\varepsilon_{cu} - \varepsilon_{ce})E_fA_f - \sigma_{pe}A_f - \left(f_y - \frac{f_u - f_y}{\varepsilon_{su} - \varepsilon_y}\right)A_s$$

$$C = -E_s'A_s'\varepsilon_{cu}a_s' - \frac{f_u - f_y}{\varepsilon_{su} - \varepsilon_y}\varepsilon_{cu}A_sh_0 - \varepsilon_{cu}E_fA_fh$$

The ultimate flexural capacity is obtained by substituting x_c the following formula is:

$$\begin{aligned} M_u &= \left(\sigma_{pe} + \varepsilon_{ce}E_f + \varepsilon_{fbu}E_f\right)A_f\left(h - \frac{x_c}{2}\right) + \sigma_sA_s\left(h_0 - \frac{x_c}{2}\right) \\ &= \left(\sigma_{pe} + \varepsilon_{ce}E_f + \varepsilon_{fbu}E_f\right)A_f\left(h - \frac{x_c}{2}\right) + \left[f_y + \frac{f_u - f_y}{\varepsilon_{su} - \varepsilon_y}\left(\varepsilon_s - \varepsilon_y\right)\right]A_s\left(h_0 - \frac{x_c}{2}\right) \end{aligned} \tag{17}$$

iii) failure mode 3

When the steel bar has not yet yielded, the carbon fibre plate has not been peeled off or broken, and the concrete in the compression zone has been crushed. Again, interpreting this condition into strain status, we have, $\varepsilon_s < \varepsilon_y$, $\varepsilon_f < \varepsilon_{fbu}$, $\varepsilon_c = \varepsilon_{cu}$, the following equation can be obtained from the plane section assumption that:

$$\varepsilon_s = \frac{h_0 - x_c}{x_c}\varepsilon_{cu} \tag{18}$$

$$\varepsilon_s' = \frac{x_c - a_s'}{x_c}\varepsilon_{cu} \tag{19}$$

$$\varepsilon_f = \frac{h - x_c}{x_c}\varepsilon_{cu} \tag{20}$$

When:

$$\sigma_s = E_s\varepsilon_s \tag{21}$$

The equation of equilibrium of the internal forces at the horizontal direction is:

$$E_s'\varepsilon_s'A_s' + F_c = \left(\sigma_{pe} + \varepsilon_{ce}E_f + \varepsilon_fE_f\right)A_f + \sigma_sA_s \tag{22}$$

By substituting Eqs. (18), (19), (20) and (21) into the equilibrium equation, Eq. (22), the expression can be simplified into the form $Ax_c^3 + Bx_c^2 + Cx_c + D = 0$, and the solution of the equation is:

$$x_c = \frac{-B - \sqrt{B^2 - 4AC}}{2A}$$

where:

$$A = \frac{b\sigma_0(3\varepsilon_{cu} + \varepsilon_0)}{3\varepsilon_{cu}}$$

$$B = E_s'A_s'\varepsilon_{cu} + E_s\varepsilon_{cu}A_s + (\varepsilon_{cu} - \varepsilon_{ce})E_fA_f - \sigma_{pe}A_f$$

$$C = -E_s'A_s'\varepsilon_{cu}a_s' - E_s\varepsilon_{cu}A_sh_0 - \varepsilon_{cu}E_fA_fh$$

The ultimate flexural capacity is obtained by substituting x_c into the following formula is:

$$M_u = \left(\sigma_{pe} + \varepsilon_{ce}E_f + \varepsilon_fE_f\right)A_f\left(h - \frac{x_c}{2}\right) + E_s\varepsilon_sA_s\left(h_0 - \frac{x_c}{2}\right) \tag{23}$$

In the above equation:

x_c- Depth of concrete compression zone.

x_0- Depth of concrete compression zone(where the edge strain of the concrete reached its ultimate compressive strain.

x- Depth of Equivalent Rectangular Stress Block ($x = \beta_1x_0$).

h- Depth of section.

h_0- Depth between the action point of tensile reinforcement and the surface of the flange plate.

σ_c- Stress of concrete.

ε_c- Strain of concrete.

σ_0- Maximum compressive stress of concrete.

ε_0- The strain value corresponds to the peak stress of concrete. The value is 0.002.

ε_{cu}- The ultimate compressive strain of concrete, the value is 0.0033.

ε_{ce}- Effective preloading strain of concrete.

A_s- Area of tension reinforcement.

A_s'- Area of compression reinforcement.

σ_s- Stress of reinforcement.

ε_s- Strain value of reinforcement.

ε_y- Yield strain of reinforcement.

ε_{su}- Ultimate tensile strain of rebar.

E_s- Elasticity modulus of reinforcement.

ε_{fbu}- Tensile strain of concrete surface (when CFRP plate reached its ultimate tensile strain).

ε_i- Initial tensile strain of CFRP plate (when the tensile strain of concrete is non-existent).

ε_f- Tensile strain without considering the initial strain of the CFRP plate.

ε_{frp}-Actual tensile strain of CFRP plate.

ε_{fu}- Ultimate tensile strain of CFRP plate.

σ_{pe}- Effective prestress of CFRP plates after loss.

σ_f-Stress of CFRP plate.

f_y-Yield strength of rebar.

f_u- Ultimate strength of rebar.

4.2.2. *Flexural capacity with shear lag effect considered*

When the shear lag effect is considered, the strain and stress distribution under bending are shown in Fig. 7. The compression zone of the box girder section, under the influence of the shear lag effect can be divided into three regions. To simplify the calculation, these regions are separated into flange component G and web component T, which consists of T1 + T2 as shown in Fig. 6.

The normal strain of the flange plate due to bending can be assumed to be the N-th order polynomial distribution along the length of the

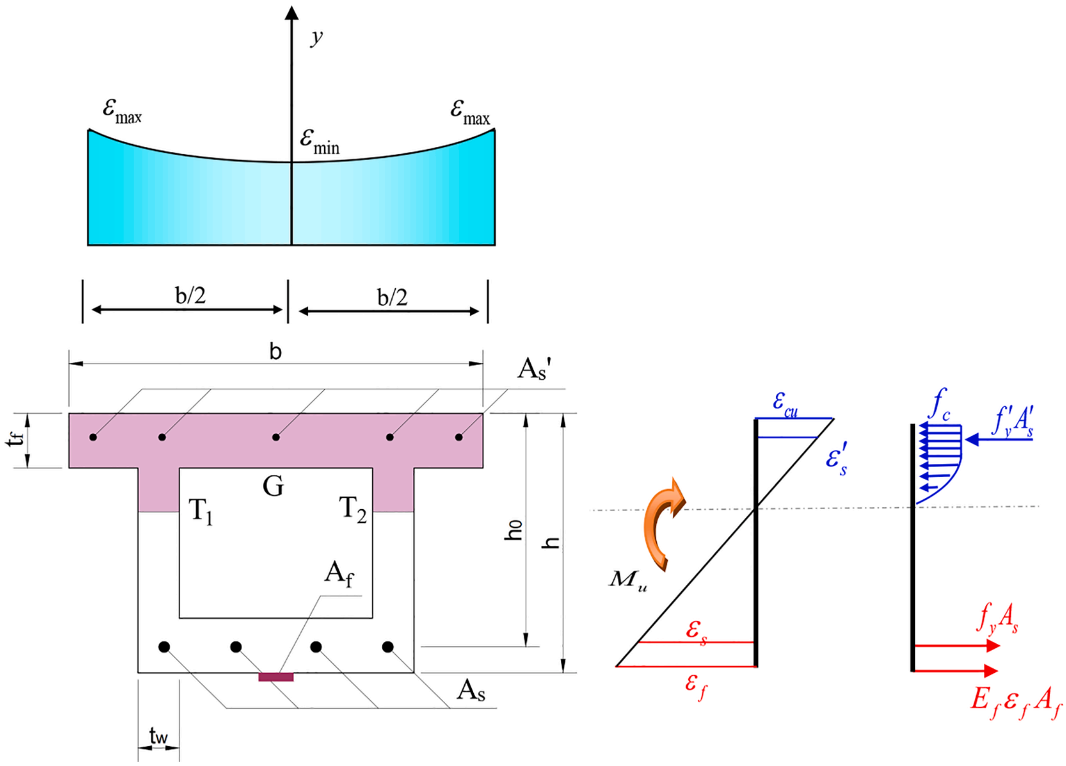

Fig. 7. Flexural capacity calculation of box girder section considering shear hysteresis effect.

beam [37,38], namely:

$$\varepsilon = \varepsilon_{\min} + (\varepsilon_{\max} - \varepsilon_{\min})\left(\frac{x}{b}\right)^N = \varepsilon_{\max}\left[\frac{1}{\alpha} + (1 - \frac{1}{\alpha})\frac{x^N}{b^N}\right] \tag{24}$$

where $\alpha = \varepsilon_{\max}/\varepsilon_{\min}$, a constant value associated with material and section configuration. Concentrated load is applied on the span of simply supported beams: $\alpha = 1 + \frac{1}{\frac{3I_G}{4I} - \frac{3kl}{7n}cth\frac{kl}{2} - 1}$, wherein: I_G is the inertia moment of the box girder flange plate to the axis x; and I is the inertia moment of the box beam full section against the axis x; $kl = \sqrt{\frac{7nl^2}{5b^2(1+\mu)}}$, $n = \frac{8I}{8I - 7I_G}$.

To consider the combining effect of the web and flange plates in different stress states: i.e., elastic, elastoplastic, and plastic stages, the following cases: Case a, Elastic range $\varepsilon_{\max} < \varepsilon_0$ and *Case b* are considered:

Case a:

If $\varepsilon_{\max} < \varepsilon_0$, the beam is still in the elastic stage, the stress and strain of the web and flange plates are shown in Fig. 8 and Fig. 9.

The resultant force, T, of the web, is:

$$T = 2\int_0^{x_c - t_f} f_c t_w \left[1 - \left(1 - \frac{\varepsilon}{\varepsilon_0}\right)^2\right] dy = 2f_c t_w \left[\frac{3\varepsilon_0\varepsilon_{\max}x_c(x_c - t_f)^2 - \varepsilon_{\max}^2(x_c - t_f)^3}{3\varepsilon_0^2 x_c^2}\right] \tag{25}$$

The moment, M_T, of the resultant web force to the neutral axis is:

$$M_T = 2\int_0^{x_c - t_f} f_c t_w \left[1 - \left(1 - \frac{\varepsilon}{\varepsilon_0}\right)^2\right] y dy = 2f_c t_w \left[\frac{8\varepsilon_0\varepsilon_{\max}x_c(x_c - t_f)^3 - 3\varepsilon_{\max}^2(x_c - t_f)^4}{12\varepsilon_0^2 x_c^2}\right] \tag{26}$$

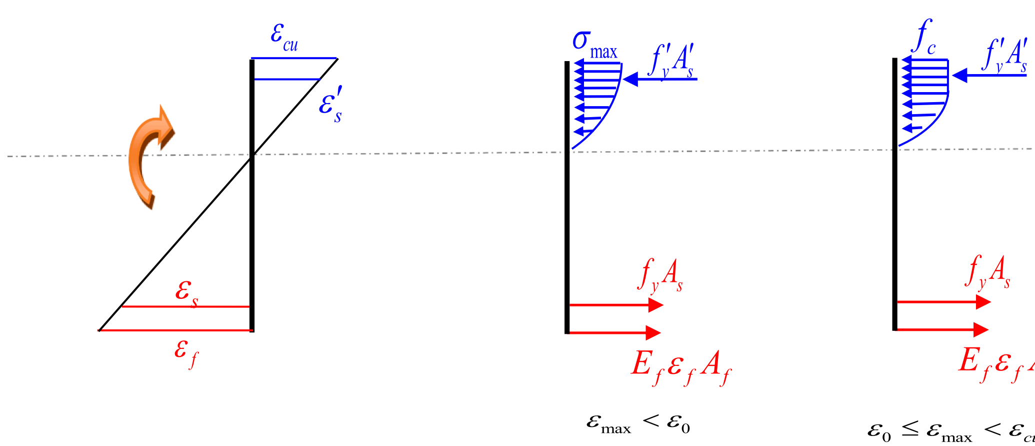

Fig. 8. Stress strain diagram of the web.

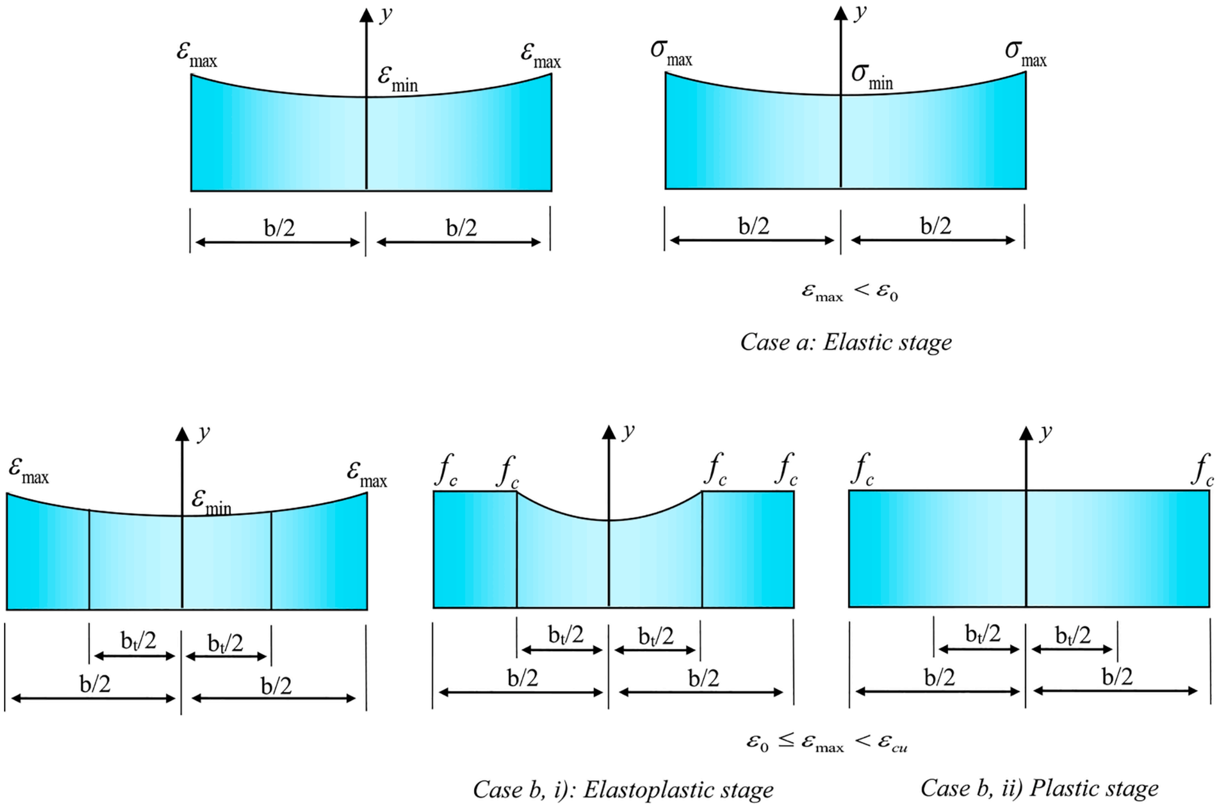

Fig. 9. The stress strain diagram of the flange plate.

The net force, G, of the flange plate, is:

$$G = 2\int_{x_c-t_f}^{x_c}\int_0^{\frac{b}{2}} f_c\left[1-\left(1-\frac{\varepsilon}{\varepsilon_0}\right)^2\right]dxdy$$
$$= f_c t_f\left\{\frac{2b\varepsilon_{max}(N+\alpha)}{\alpha\varepsilon_0(N+1)} - \frac{b\varepsilon_{max}^2}{\alpha^2\varepsilon_0^2}\left[\frac{N+2\alpha-1}{N+1}+\frac{(\alpha-1)^2}{2N+1}\right]\right\} \tag{27}$$

The resultant moment, M_G, of the flange plate to the neutral axis is:

$$M_G = 2\int_{x_c-t_f}^{x_c}\int_0^{\frac{b}{2}} f_c\left[1-\left(1-\frac{\varepsilon}{\varepsilon_0}\right)^2\right]ydxdy$$
$$= f_c t_f(2x_c-t_f)\left\{\frac{b\varepsilon_{max}(N+\alpha)}{\alpha\varepsilon_0(N+1)} - \frac{b\varepsilon_{max}^2}{2\alpha^2\varepsilon_0^2}\left[\frac{N+2\alpha-1}{N+1}+\frac{(\alpha-1)^2}{2N+1}\right]\right\} \tag{28}$$

Case b:

If $\varepsilon_0 < \varepsilon_{max} < \varepsilon_{cu}$, the beam may be in the elastic–plastic stage or the plastic stage, and the stress and strain of the flange plate are shown in Fig. 9.

(i) When $\varepsilon_{min} < \varepsilon_0$, namely $\sigma_{min} < f_c$, the beam is in the elastic–plastic stage, where there are both elastic and plastic regions.

Assume that half of the elastic zone width is b_t, then:

$$b_t = k_f\frac{b}{2} \tag{29}$$

In the formula k_f is the coefficient of the elastic region, $0 \leqslant k_f \leqslant 1$.

When $x = b_t$, that is $x = k_f\frac{b}{2}$, $\varepsilon = \varepsilon_0$, k_f can be obtained by substituting into the formula that:

$$k_f = \sqrt[N]{\frac{\alpha\varepsilon_0 - \varepsilon_{max}}{(\alpha-1)\varepsilon_{max}}} \tag{30}$$

It is important to understand the influence of α on k_f and b_t: for a certain member, when the reinforcement, load and section size are fixed, α is constant. However, α affects the determination of value k_f, sequentially affecting the determination of value b_t. In the case of $\varepsilon_0 < \varepsilon_{max} \leqslant \varepsilon_{cu}$ when ε_{max} is certain, if k_f is greater than 0, it indicates the existence of an elastic zone; if k_f is equal to 0, it means that there is no elastic zone and the member is in the plastic stage while $\alpha = \frac{\varepsilon_{max}}{\varepsilon_0}$.

The net force, T, of the web is:

$$T = 2\int_0^{x_1} f_c t_w\left[1-\left(1-\frac{\varepsilon}{\varepsilon_0}\right)^2\right]dy + 2f_c t_w(x_c - t_f - x_1)$$
$$= 2f_c t_w\left[x_c - t_f - \frac{x_c\varepsilon_0}{3\varepsilon_{max}}\right] \tag{31}$$

x_1 is the depth of the concrete compression zone where the compressive stress of concrete does not reach its peak stress.

The resultant web moment, M_T, to the neutral axis is:

$$M_T = 2\int_0^{x_1} f_c t_w\left[1-\left(1-\frac{\varepsilon}{\varepsilon_0}\right)^2\right]ydy + f_c t_w(x_c - t_f - x_1)(x_c - t_f + x_1)$$
$$= f_c t_w\left[(x_c - t_f)^2 - \frac{x_c^2\varepsilon_0^2}{6\varepsilon_{max}^2}\right] \tag{32}$$

Generally,

$$x_1 = \frac{\varepsilon_0}{\varepsilon_{max}}x_c \tag{33}$$

The net force, G, of the flange plate, is:

$$G = 2\int_{x_c-t_f}^{x_c}\int_0^{b_t} f_c\left[1-\left(1-\frac{\varepsilon}{\varepsilon_0}\right)^2\right]dxdy + 2f_c t_f\left(\frac{b}{2}-b_t\right)$$
$$= 2f_c t_f\left\{\frac{b\varepsilon_{max}k_f}{2\alpha\varepsilon_0}\left[1+\frac{(\alpha-1)k_f^N}{N+1}\right] - \frac{b\varepsilon_{max}^2 k_f}{2\alpha^2\varepsilon_0^2}\left[1+\frac{2(\alpha-1)k_f^N}{N+1}+\frac{(\alpha-1)^2k_f^N}{2N+1}\right]\right\}$$
$$+ bf_c t_f(1-k_f) \tag{34}$$

The resultant moment, M_G, of the flange plate to the neutral axis is:

$$M_G = 2\int_{x_c-t_f}^{x_c}\int_0^{b_t} f_c\left[1-\left(1-\frac{\varepsilon}{\varepsilon_0}\right)^2\right]dxdy + 2f_ct_f\left(\frac{b}{2}-b_t\right)(x_c-t_f)$$
$$= f_ct_f(2x_c-t_f)\left\{\frac{2b\varepsilon_{\max}(N+\alpha)}{\alpha\varepsilon_0(N+1)} - \frac{b\varepsilon_{\max}^2}{\alpha^2\varepsilon_0^2}\left[\frac{N+2\alpha-1}{N+1}+\frac{(\alpha-1)^2}{2N+1}\right]\right\} + bf_ct_f(1-k_f)(2x_c-t_f) \tag{35}$$

(ii) When $\varepsilon_{\min}\geqslant\varepsilon_0$, that is $\sigma_{\min} = f_c$, the beam is in a completely plastic stage when $k_f = 0$. Substitute $k_f = 0$ into each formula above.

The net force, T, of the web, is:

$$T = 2\int_0^{x_1} f_ct_w\left[1-\left(1-\frac{\varepsilon}{\varepsilon_0}\right)^2\right]dy + 2f_ct_w(x_c-t_f-x_1) = 2f_ct_w\left[x_c-t_f-\frac{x_c\varepsilon_0}{3\varepsilon_{\max}}\right] \tag{36}$$

The resultant moment, M_T, of the web to the neutral axis is:

$$M_T = 2\int_0^{x_1} f_ct_w\left[1-\left(1-\frac{\varepsilon}{\varepsilon_0}\right)^2\right]ydy + 2f_ct_w\cdot(x_c-t_f-x_1)\cdot\frac{1}{2}(x_c-t_f+x_1) = f_ct_w\cdot\left[(x_c-t_f)^2-\frac{x_c^2\varepsilon_0^2}{6\varepsilon_{\max}^2}\right] \tag{37}$$

The net force, G, of the flange plate, is:

$$G = f_cbt_f \tag{38}$$

The resultant moment, M_G, of the flange plate to the neutral axis is:

$$M_G = f_cbt_f(x_c-t_f) \tag{39}$$

Similar to the previous approach, three failure modes are considered:

i) failure mode 1

The steel has yielded, the concrete has not been crushed, and the carbon fibre plate has reached its ultimate tensile strain and been pulled apart.

According to the plane section assumption, there is:

$$\varepsilon_c = \frac{x_c}{h-x_c}\varepsilon_{cu} \tag{40}$$

$$\varepsilon_{cu} = \frac{h-x_c}{x_c}\varepsilon_{\max} \tag{41}$$

$$\varepsilon_s' = \frac{x_c-a_s'}{x_c}\varepsilon_{\max} \tag{42}$$

Moreover,

$$k_f = \sqrt[N]{\frac{\alpha\varepsilon_0-\varepsilon_{\max}}{(\alpha-1)\varepsilon_{\max}}} \tag{43}$$

(a) When the strain of the concrete edge in the compression zone has not reached the peak strain, that is $\varepsilon_{\max} < \varepsilon_0$; $\varepsilon_s'\geqslant\varepsilon_y'$, $\sigma_s'\geqslant\sigma_y'$;$\varepsilon_s\geqslant\varepsilon_y$,$\sigma_s = f_y$;$\varepsilon_f = \varepsilon_{fu}$, $\sigma_f = f_{fu}$.

The net force, T, of the web, is:

$$T = 2f_ct_w\left[\frac{3\varepsilon_0\varepsilon_{\max}x_c(x_c-t_f)^2-\varepsilon_{\max}^2(x_c-t_f)^3}{3\varepsilon_0^2x_c^2}\right] \tag{44}$$

The resultant moment, M_T, of the web to the neutral axis is:

$$M_T = 2f_ct_w\left[\frac{8\varepsilon_0\varepsilon_{\max}x_c(x_c-t_f)^3-3\varepsilon_{\max}^2(x_c-t_f)^4}{12\varepsilon_0^2x_c^2}\right] \tag{45}$$

The net force, G, of the flange plate, is:

$$G = 2f_ct_f\left\{\frac{b\varepsilon_{\max}(N+\alpha)}{\alpha\varepsilon_0(N+1)} - \frac{b\varepsilon_{\max}^2}{2\alpha^2\varepsilon_0^2}\left[\frac{N+2\alpha-1}{N+1}+\frac{(\alpha-1)^2}{2N+1}\right]\right\} \tag{46}$$

The resultant moment, M_G, of the flange plate to the neutral axis is:

$$M_G = \left\{\frac{b\varepsilon_{\max}(N+\alpha)}{\alpha\varepsilon_0(N+1)} - \frac{b\varepsilon_{\max}^2}{2\alpha^2\varepsilon_0^2}\left[\frac{N+2\alpha-1}{N+1}+\frac{(\alpha-1)^2}{2N+1}\right]\right\}f_ct_f(2x_c-t_f) \tag{47}$$

From the axial force equilibrium condition:

$$G+T+E_s\varepsilon_s'A_s' = E_f\varepsilon_{fu}A_f+f_yA_s \tag{48}$$

Combining Eqs. (40), (41), (42), (44), (46) and (48), the height x_c of the compression zone, the strain ε_s' of the reinforcement in the compression zone, and the strain ε_{fu} of the CFRP plate can be obtained. The ultimate flexural bearing capacity can be reached by taking the moment of neutral axis:

$$M_u = M_T+M_G+f_yA_s(h_0-x_c)+E_f\varepsilon_{fu}A_f(h-x_c)+E_s\varepsilon_sA_s'(x_c-a_s') \tag{49}$$

(b) The strain of the concrete edge in the compression zone has reached the peak strain, that is $\varepsilon_{cu} > \varepsilon_{\max} > \varepsilon_0$, $\varepsilon_s'\geqslant\varepsilon_y'$, $\sigma_s'\geqslant\sigma_y'$, $\varepsilon_s\geqslant\varepsilon_y$, $\sigma_s = f_y$, $\varepsilon_f = \varepsilon_{fbu}$, $\sigma_f = f_{fu}$.

The net force, T, of the web, is:

$$T = 2f_ct_w\left[x_c-t_f-\frac{x_c\varepsilon_0}{3\varepsilon_{\max}}\right] \tag{50}$$

The resultant moment, M_T MT, of the web to the neutral axis is:

$$M_T = f_ct_w\left[(x_c-t_f)^2-\frac{x_c^2\varepsilon_0^2}{6\varepsilon_{\max}^2}\right] \tag{51}$$

The net force, G, of the flange plate, is:

$$G = 2f_ct_f\left\{\frac{b\varepsilon_{\max}k_f}{\alpha\varepsilon_0}\left[1+\frac{(\alpha-1)k_f^N}{N+1}\right] - \frac{b\varepsilon_{\max}^2k_f}{\alpha^2\varepsilon_0^2}\left[1+\frac{2(\alpha-1)k_f^N}{N+1}+\frac{(\alpha-1)^2k_f^N}{2N+1}\right]\right\} + bf_ct_f(1-k_f) \tag{52}$$

The resultant moment, M_G, of the flange plate to the neutral axis is:

$$M_G = f_ct_f(2x_c-t_f)\left\{\frac{b\varepsilon_{\max}(N+\alpha)}{\alpha\varepsilon_0(N+1)} - \frac{b\varepsilon_{\max}^2}{2\alpha^2\varepsilon_0^2}\left[\frac{N+2\alpha-1}{N+1}+\frac{(\alpha-1)^2}{2N+1}\right]\right\} + bf_ct_f(1-k_f)(2x_c-t_f) \tag{53}$$

From the axial force equilibrium condition:

$$G+T+E_s\varepsilon_s'A_s' = E_f\varepsilon_{fu}A_f+f_yA_s \tag{54}$$

Eqs. (50), (52), (54) can be combined to obtain the height x_c of the compression zone, the strain ε_s' of the reinforcement in the compression zone and the strain ε_{fu} of the CFRP plate. The ultimate flexural capacity can be obtained by taking the moment of the neutral axis:

$$M_u = M_T+M_G+f_yA_s(h_0-x_c)+E_f\varepsilon_{fu}A_f(h-x_c)+E_s\varepsilon_sA_s'(x_c-a_s') \tag{55}$$

ii) failure mode 2

The steel bar has yielded, the CFRP plate has not reached the ultimate tensile strain and been broken, and the concrete is crushed.

The strain of the concrete edge in the compression zone has reached the strain limit, that is

$$\varepsilon_c = \varepsilon_{cu}\varepsilon_s'\geqslant\varepsilon_y'\sigma_s'\geqslant\sigma_y'\varepsilon_s\geqslant\varepsilon_y\sigma_s = f_y\varepsilon_f < \varepsilon_{fbu}\sigma_f < f_{fu}$$

According to the plane section assumption, there is:

$$\varepsilon_f = \frac{h-x_c}{x_c}\varepsilon_{cu} \tag{56}$$

The net force, T, of the web, is:

$$T = 2f_c t_w\left[x_c - t_f - \frac{x_c\varepsilon_0}{3\varepsilon_{\max}}\right] \tag{57}$$

The resultant moment, M_T, of the web to the neutral axis is:

$$M_T = f_c t_w\left[\left(x_c - t_f\right)^2 - \frac{x_c^2\varepsilon_0^2}{6\varepsilon_{\max}^2}\right] \tag{58}$$

The net force, G, of the flange plate, is:

$$G = 2f_c t_f\left\{\frac{b\varepsilon_{\max}k_f}{\alpha\varepsilon_0}\left[1+\frac{(\alpha-1)k_f^N}{N+1}\right] - \frac{b\varepsilon_{\max}^2 k_f}{\alpha^2\varepsilon_0^2}\left[1+\frac{2(\alpha-1)k_f^N}{N+1}+\frac{(\alpha-1)^2k_f^N}{2N+1}\right]\right\} + bf_c t_f(1-k_f) \tag{59}$$

The resultant moment, M_G, of the flange plate to the neutral axis is:

$$M_G = f_c t_f(2x_c - t_f)\left\{\frac{2b\varepsilon_{\max}(N+\alpha)}{\alpha\varepsilon_0(N+1)} - \frac{b\varepsilon_{\max}^2}{\alpha^2\varepsilon_0^2}\left[\frac{N+2\alpha-1}{N+1}+\frac{(\alpha-1)^2}{2N+1}\right]\right\} + bf_c t_f(1-k_f)(2x_c - t_f) \tag{60}$$

From the axial force equilibrium condition:

$$G + T + f_y^{'}A_s^{'} = \sigma_f A_f + f_y A_s \tag{61}$$

By combining Eqs. (56), (57), (59) and (61), the height x_c of the compression zone and the strain $\varepsilon_s^{'}$ of the reinforcement in the compression zone can be reached. The ultimate flexural bearing capacity can be obtained by taking the moment of the neutral axis:

$$M_u = M_T + M_G + f_y A_s(h_0 - x_c) + \sigma_f A_f(h - x_c) + f_y^{'}A_s^{'}(x_c - a_s^{'}) \tag{62}$$

iii) failure mode 3

The steel bars have not yielded, the CFRP plates have not been stripped or broken, and the concrete in the compression zone is crushed.

The strain of the concrete edge in the compression zone has reached the strain limit, that is

$$\varepsilon_c = \varepsilon_{cu}\varepsilon_s^{'} \geqslant \varepsilon_y^{'}\sigma_s^{'} \geqslant \sigma_y^{'}\varepsilon_s < \varepsilon_y\sigma_s = E_s\varepsilon_s\varepsilon_f < \varepsilon_{fbu}\sigma_f = E_f\varepsilon_{frp} \;=\; E_f\left(\varepsilon_f + \varepsilon_i\right)$$

According to the plane section assumption:

$$\varepsilon_s = \frac{h_0 - x_c}{x_c}\varepsilon_{cu} \tag{63}$$

$$\varepsilon_f = \frac{h - x_c}{x_c}\varepsilon_{cu} \tag{64}$$

The net force, T, of the web, is:

$$T = 2f_c t_w\left[x_c - t_f - \frac{x_c\varepsilon_0}{3\varepsilon_{\max}}\right] \tag{65}$$

The resultant moment, M_T, of the web to the neutral axis is:

$$M_T = f_c t_w\left[\left(x_c - t_f\right)^2 - \frac{x_c^2\varepsilon_0^2}{6\varepsilon_{\max}^2}\right] \tag{66}$$

The net force, G, of the flange plate, is:

$$G = 2f_c t_f\left\{\frac{b\varepsilon_{\max}k_f}{\alpha\varepsilon_0}\left[1+\frac{(\alpha-1)k_f^N}{N+1}\right] - \frac{b\varepsilon_{\max}^2 k_f}{\alpha^2\varepsilon_0^2}\left[1+\frac{2(\alpha-1)k_f^N}{N+1}+\frac{(\alpha-1)^2k_f^N}{2N+1}\right]\right\} + bf_c t_f(1-k_f) \tag{67}$$

The resultant moment, M_G, of the flange plate to the neutral axis is:

$$M_G = f_c t_f(2x_c - t_f)\left\{\frac{b\varepsilon_{\max}(N+\alpha)}{\alpha\varepsilon_0(N+1)} - \frac{b\varepsilon_{\max}^2}{\alpha^2\varepsilon_0^2}\left[\frac{N+2\alpha-1}{N+1}+\frac{(\alpha-1)^2}{2N+1}\right]\right\} + bf_c t_f(1-k_f)(x_c - \frac{t_f}{2}) \tag{68}$$

From the axial force equilibrium condition:

$$G + T + f_y^{'}A_s^{'} = \sigma_f A_f + f_y A_s \tag{69}$$

Eqs. (63), (64), (65), (67) and (69) can be combined to obtain the height x_c of the compression zone, the strain $\varepsilon_s^{'}$ of the reinforcement in the compression zone and the strain ε_{fu} of the CFRP plate. The ultimate flexural capacity, M_u; can be obtained by taking the moment of the neutral axis:

$$M_u = M_T + M_G + E_s\varepsilon_s A_s(h_0 - x_c) + E_f\varepsilon_{frp}A_f(h - x_c) + f_y^{'}A_s^{'}(x_c - a_s^{'}) \tag{70}$$

To verify the proposed analytical expression for the flexural capacity of the two box girders, the theoretical calculation values were obtained using the theoretical equations derived under the different failure modes discussed previously. The theoretical values were then compared with the experimental values, as shown in Table 6.

Table 7 shows that the difference between the experimental flexural capacity and the theoretical one is only 3% for the concrete box beam reinforced with prestressed CFRP plates, and the maximum difference is only 4%. The results show that the theoretical values agree with the experimental values.

5. Conclusion

This paper proposes an analytical model for analysing and designing the RC concrete box girders strengthened by prestressed CFRP plates. A complementary experimental study validated the performance of the proposed analytical model. The analytical predictions of the ultimate loads for RC concrete box girders with different design configurations agreed well with the experimental results. Furthermore, it was found that the proposed model is practical and applicable to different design configurations and can handle different failure modes in practical applications.

The proposed method for estimating the partial prestress loss accurately predicted the total press loss. Moreover, the estimations agreed well with the total prestress loss measured by the strain gauges. Also, the test results showed that most of the prestress losses occurred during the adhesive curing stage (generally within the first 15 days after tension).

In addition to the prestress loss, the proposed analytical model also considered the shear lag effect and failure modes under different design configurations at elastic, elastoplastic and plastic stages. This study executed a complete analytical work for analysing and designing complex new or aged RC box girders strengthened by the prestressed CFRP plates.

CRediT authorship contribution statement

Yu Deng: Conceptualization, Data curation, Formal analysis, Funding acquisition, Investigation, Methodology, Project administration,

Table 7
Comparison of experimental value and analytical prediction of ultimate load.

Specimen number	Ultimate load test value/kN	Theoretical calculation of ultimate load/kN	Test value/ calculation value
DBL	318	320.2	0.99
JGL1-3P	453	436.5	1.04
JGL1-4P	469	459.2	1.02
JGL2-4P	548	532.7	1.03
JGL3-3P	505	492.3	1.03
JGL3-4P	515	503.5	1.02
SSL1A-3P	450	440.2	1.02
SSL1B-4P	449	457.5	0.98

Resources, Supervision, Validation, Visualization, Writing – original draft, Writing – review & editing. **Daoyuan Ling:** Data curation, Formal analysis, Investigation, Methodology, Software, Validation, Visualization, Writing – original draft, Writing – review & editing. **Zhen Guo:** Data curation, Formal analysis, Investigation, Methodology, Software, Validation, Visualization, Writing – original draft, Writing – review & editing. **Piti Sukontasukkul:** Formal analysis, Investigation, Methodology, Validation, Writing – original draft, Writing – review & editing. **Terry Y.P. Yuen:** Formal analysis, Investigation, Methodology, Validation, Writing – original draft, Writing – review & editing. **Simon H.F. Wong:** Formal analysis, Methodology, Validation, Writing – original draft, Writing – review & editing. **Mark Adom-Asamoah:** Formal analysis, Methodology, Validation, Writing – original draft, Writing – review & editing. **Suchart Limkatanyu:** Formal analysis, Methodology, Validation, Writing – original draft, Writing – review & editing. **Chayanon Hansapinyo:** Formal analysis, Methodology, Validation, Writing – original draft, Writing – review & editing. **Jack Banahene Osei:** Validation, Writing – original draft, Writing – review & editing. **Jones Owusu-Twumasi:** Validation, Writing – original draft, Writing – review & editing. **J.S. Kuang:** Validation, Writing – original draft, Writing – review & editing. **Hexin Zhang:** Conceptualization, Funding acquisition, Investigation, Methodology, Project administration, Resources, Supervision, Writing – original draft, Writing – review & editing.

Declaration of Competing Interest

The authors declare that they have no known competing financial interests or personal relationships that could have appeared to influence the work reported in this paper.

Data availability

No data was used for the research described in the article.

Acknowledgements

This research was supported/partially supported by the Royal Academy of Engineering-Industrial Fellowship (IF\192023), National Nature Science Foundation of China (51768008, 52168016), British Council and Ministry of Education, China (UK-China-BRI Countries Education Partnership Initiative 2019), British Council (Enabling Grants to Strengthen UK-China Institutional Partnerships through academic collaboration 2021), Nature Science Foundation of Guangxi Zhuang Autonomous Region (2019JJA160137), and Royal Academy of Engineering-Visiting Professor (VP2021\7\12).

References

[1] Shahawy M, Beitelman T. Flexural behavior of reinforced concrete beams strengthened with advanced composite materials. Covina, CA: Society for the Advancement of Material and Process Engineering; 1996.
[2] Deng Y, Li Z, Zhang H, Corigliano A, Lam ACC, Hansapinyo C, et al. Experimental and analytical investigation on flexural behaviour of RC beams strengthened with NSM CFRP prestressed concrete prisms. Compos Struct 2021;257:113385.
[3] Deng Y, Ma F, Zhang H, Wong SHF, Pankaj P, Zhu L, et al. Experimental study on shear performance of RC beams strengthened with NSM CFRP prestressed concrete prisms. Eng Struct 2021;235:112004.
[4] Deng Y, Shen M, Zhang H, Zhang P, Yuen TYP, Hansapinyo C, et al. Experimental and analytical studies on steel-reinforced concrete composite members with bonded prestressed CFRP tendon under eccentric tension. Compos Struct 2021;271:114124.
[5] Deng Y, Gui J, Zhang H, Taliercio A, Zhang P, Wong SHF, et al. Study on crack width and crack resistance of eccentrically tensioned steel-reinforced concrete members prestressed by CFRP tendons. Eng Struct 2022;252:113651.
[6] Haryanto Y, Hu H-T, Han Ay L, Hsiao F-P, Teng C-J, Hidayat Banu A, et al. Numerical investigation on RC T-beams strengthened in the negative moment region using NSM FRP rods at various depth of embedment. Comput Concr 2021;28:347–60.
[7] Halder R, Yuen TYP, Chen W-W, Zhou X, Deb T, Zhang H, et al. Tendon stress evaluation of unbonded post-tensioned concrete segmental bridges with two-variable response surfaces. Eng Struct 2021;245:112984.
[8] Zheng Y, Zhou N, Zhou L, Zhang H, Li H, Zhou Y. Experimental and theoretical study of bond behaviour between FRP bar and high-volume fly ash-self-compacting concrete. Mater Struct 2021;54:27.
[9] Tang Y, Huang Z, Chen Z, Chen M, Zhou H, Zhang H, et al. Novel visual crack width measurement based on backbone double-scale features for improved detection automation. Eng Struct 2023;274:115158.
[10] Intarabut D, Sukontasukkul P, Phoo-ngernkham T, Zhang H, Yoo D-Y, Limkatanyu S, et al. Influence of graphene oxide nanoparticles on bond-slip reponses between fiber and geopolymer mortar. Nanomaterials 2022.
[11] Hansapinyo C, Limkatanyu S, Zhang H, Imjai T. Residual strength of reinforced concrete beams under sequential small impact loads. Buildings 2021.
[12] Pongsopha P, Sukontasukkul P, Zhang H, Limkatanyu S. Thermal and acoustic properties of sustainable structural lightweight aggregate rubberized concrete. Results Eng 2022;13:100333.
[13] Feng W, Tang Y, Yang Y, Cheng Y, Qiu J, Zhang H, et al. Mechanical behavior and constitutive model of sustainable concrete: Seawater and sea-sand recycled aggregate concrete. Constr Build Mater 2023;364:130010.
[14] Wight R, Green M, Erki M. Post-strengthening prestressed concrete beams with prestressed FRP sheets. Proceedings of the 2ND international conference on advanced composite materials in bridges and structures, ACMBS-II, MONTREAL 19961996.
[15] Bansal PP, Sharma R, Mehta A. Retrofitting of RC girders using pre-stressed CFRP sheets. Steel Compos Struct 2016;20:833–49.
[16] Garden HN, Hollaway L. An experimental study of the strengthening of reinforced concrete beams using prestressed carbon composite plates. PROCEEDINGS OF THE SEVENTH INTERNATIONAL CONFERENCE ON STRUCTURAL FAULTS AND REPAIR, : Structural faults + repair. 1997.
[17] Garden HN, Hollaway LC. An experimental study of the failure modes of reinforced concrete beams strengthened with prestressed carbon composite plates. Compos B Eng 1998;29:411–24.
[18] Li X, Deng J, Wang Y, Xie Y, Liu T, Rashid K. RC beams strengthened by prestressed CFRP plate subjected to sustained loading and continuous wetting condition: Time-dependent prestress loss. Constr Build Mater 2021;275:122187.
[19] Yang D-S, Park S-K, Neale KW. Flexural behaviour of reinforced concrete beams strengthened with prestressed carbon composites. Compos Struct 2009;88:497–508.
[20] Ahmed E, Sobuz HR, Sutan NM. Flexural performance of CFRP strengthened RC beams with different degrees of strengthening schemes. Int J Phys Sci 2011;6:2229–38.
[21] Weichen X, Yuan T, Xiaohui W. Calculation methods for flexural capacity of normal section of concrete beams prestressed with bonded FRP tendons [J]. Build Struct 2008;3.
[22] Emdad R, Al-Mahaidi R. Effect of prestressed CFRP patches on crack growth of centre-notched steel plates. Compos Struct 2015;123:109–22.
[23] Zhang W. Experimental and Theoretical Study of T Beams Strengthened With High Prestressed CFRP Plate. Chongqing: Chongqing Jiaotong University; 2013.
[24] Choi Han T, West Jeffrey S, Soudki KA. Analysis of the flexural behavior of partially bonded FRP strengthened concrete beams. J Compos Constr 2008;12:375–86.
[25] Täljsten B. Strengthening of beams by plate bonding. J Mater Civ Eng 1997;9:206–12.
[26] Deng J, Lee MMK. Effect of plate end and adhesive spew geometries on stresses in retrofitted beams bonded with a CFRP plate. Compos B Eng 2008;39:731–9.
[27] Woo S-K, Nam J-W, Kim J-H-J, Han S-H, Byun KJ. Suggestion of flexural capacity evaluation and prediction of prestressed CFRP strengthened design. Eng Struct 2008;30:3751–63.
[28] Yang M, Hu Y, Zhang J, Ding G, Song C. Analytical model for flexural damping responses of CFRP cantilever beams in the low-frequency vibration. J Low Freq Noise Vibrat Active Control 2018;37:669–81.
[29] Chaallal O, Mofidi A, Benmokrane B, Neale K. Embedded through-section FRP rod method for shear strengthening of RC beams: performance and comparison with existing techniques. J Compos Constr 2011;15:374–83.
[30] Peng H, Shang S-p, Jin Y-j, Wang M. Experimental study of reinforced concrete beam with prestressed CFRP plate [J]. Eng Mech 2008;5.
[31] China NSotPsRo. JTG/T J22-2008: Specifications for Strengthening Design of Highway Bridges. Ministry of Housing and Urban-Rural Development of PRC; 2008.
[32] China NSotPsRo. GB 50367-2013: Code for design of strengthening concrete structure. Ministry of Housing and Urban-Rural Development of the PRC; 2013.
[33] China NSotPsRo. CECS 146-2003: Technical specification for strengthening concrete structures with carbon fiber reinforced polymer laminate. China Engineering Construction Standardization Association; 2003.
[34] Committee ACI, American Concrete I. ACI 440. 2R-17 Guide for the Design and Construction of Externally Bonded FRP Systems for Strengthening Concrete Structures: American Concrete Institute, 2017.
[35] Deng L, Chen H, Zhang P. Study on calculation methods for flexural capacity of normal section of concrete beams strengthened with prestressed CFRP plates. Build Sci 2009;1:4.
[36] Deng L, Zhang P, Yang F, Kang K. Study on prestress lost of concrete structure strenthened with prestressed CFRP plates. Ind Constr 2012;3:71–4.
[37] Wu Y, Lai Y. Elastic-plastic ultimate strength analysis of thin-walled steel box Girder with shear lag effect. Eng Mech 1997;3:319–23.
[38] Zhou S-J. Shear lag analysis of box girders. Eng Mech 2008;18:33–8.